Nuclear Instruments and Methods in Physics Research A 629 (2011) 87–92

Contents lists available at ScienceDirect

Nuclear Instruments and Methods in Physics Research A

journal homepage: www.elsevier.com/locate/nima

A GEANT4-based simulation model for the BESIII endcap time-of-flight system

Y. Liu [a,b,*], Z.Y. Deng [a], H.M. Liu [a], S.S. Sun [a], H.L. Tian [a,b], Y.F. Wang [a], X.J. Zhang [a,b], C. Zhao [a,c]

[a] Institute of High Energy Physics, Chinese Academy of Sciences, Beijing 100049, China
[b] Graduate University of Chinese Academy of Sciences, Beijing 100049, China
[c] Department of Modern Physics, University of Science and Technology of China, Hefei 230026, China

ARTICLE INFO

Article history:
Received 11 August 2010
Received in revised form
2 November 2010
Accepted 17 November 2010
Available online 25 November 2010

Keywords:
Detector simulation
Time-of-flight (TOF)
Optical photon
GEANT
BESIII

ABSTRACT

A GEANT4-based full Monte-Carlo model is developed to simulate the performance of the endcap time-of-flight (TOF) system of the BESIII detector with high accuracy and sufficient speed. Experimental data of e^+e^- collisions collected at BESIII are used to test this model, which can also be applied to other cases for precisely simulating optical photons propagating in scintillators with an irregular geometry.

1. Introduction

BESIII [1] is a new spectrometer located at the upgraded Beijing Electron Positron Collider (BEPCII), which runs in the τ−charm physics [2] energy region ($\sqrt{s}=2-4.6$ GeV). One of the sub-detectors, the time-of-flight (TOF) system used for trigger and particle identification (PID), is made of plastic scintillators arranged to form a barrel and two endcaps. Reliable Monte-Carlo (MC) simulation plays an important role in understanding the TOF system and minimizing systematic uncertainties in physics analysis. It is therefore desirable to build a precise simulation model based on first principles and physical laws, rather than parameterised models inferred from experimental data [3]. We choose to base the model on GEANT4 [4,5] and it should incorporate all physics processes related to the generation and propagation of optical photons (photons with the wavelengths much greater than the typical atomic spacing) in scintillators, the optical and electrical signal generation in photomultiplier tubes (PMT), the electrical signal propagation and processing in the readout electronics and the mixing of the signal with beam-related backgrounds.

A full simulation of a large number (of order 10^9) of e^+e^- collisions ('events') would require huge computing resources, given that each event requires the simulation of a large number (up to 10^5) of optical photons resulting from the interactions of primary and secondary particles with the detector material. For scintillators with simple shapes of high symmetry, an optical method [6], based on an analytical calculation, was developed to speed up the simulation. However, this method fails for the more complicated geometry of the BESIII endcap TOF [7–9]. The MC code PHOTON [10] supports simulation of optical photons in an arbitrarily complex geometry, but it is independent of GEANT4. In this letter, we report our efforts trying to fully simulate optical photon processes in a complicated geometry using GEANT4. To some extent, our motivation and the solution are similar to the fast simulation for calorimeters used by many experiments [11,12]. This GEANT4-based simulation model is applied successfully to the endcap TOF and meets the requirements in both accuracy and speed for the BESIII experiment, where billions of MC events have to be produced every year using the BESIII Object-Oriented Simulation Tool (BOOST) [13].

2. Geometry and material of the endcap TOF system

The endcap TOF system consists of twice 48 plastic scintillators (BICRON BC404 [14]), located at the east and west side, respectively, 1330 mm away from the interaction point (IP) along the beam direction (chosen as the $\hat{z}$ axis in the global BESIII coordinate system), covering polar angles from 18.2° to 31.8° in the east side and from 148.2° to 161.8° in the west side. Its structure is shown in Fig. 1(a). For each single scintillator, as shown in Fig. 1(b), the length of the trapezoid is 431 mm and the thickness is 48 mm. Widths of top and bottom sides are 116.5 and 53.7 mm, respectively. The center of a photomultiplier tube (PMT, Hamamatsu R5924 [15]) is

* Corresponding author at: Institute of High Energy Physics, Chinese Academy of Sciences, Beijing 100049, China. Tel.: +86 108823 6510; fax: +86 108823 3083.
E-mail addresses: liuyong1001@gmail.com, liuyong@ihep.ac.cn (Y. Liu).

0168-9002/$ - see front matter © 2010 Elsevier B.V. All rights reserved.
doi:10.1016/j.nima.2010.11.098

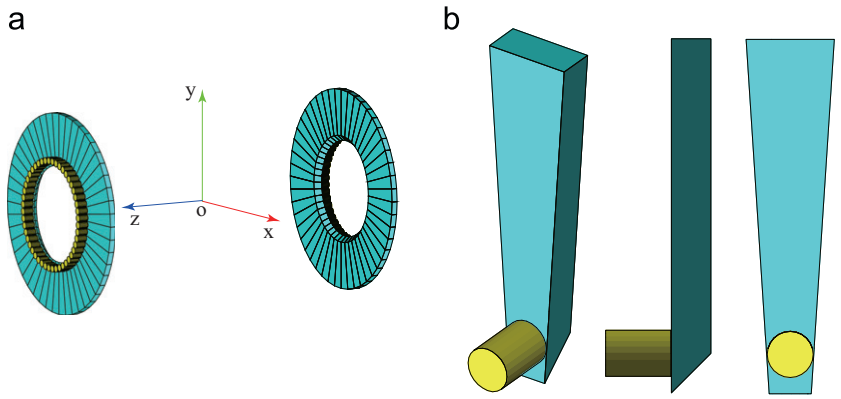

Fig. 1. The geometry of the endcap TOF; (a) The endcap TOF system in the BESIII; (b) A single scintillator from different angles of view.

Table 1
The Property of Scintillator BC404.

Light yield	Rise time	Decay time	Pulse width (FWHM)	Refractive index	Bulk light attenuation length
8500 photons/MeV	0.7 ns	1.8 ns	2.2 ns	1.58	1600 mm

placed 48 mm from the bottom and coupled to the scintillator by an optical interface pad (BICRON BC-634A [16]). For better photon collection efficiency, the bottom side is sloped at an angle of 45°. Each scintillator is wrapped with enhanced specular reflector (ESR) film with an average reflectivity of 98.5% (for wavelengths (λ) of photons in the region $390 \leq \lambda \leq 500$ nm [17]).

3. GEANT4-based simulation model

The full simulation, including the exact description of the geometry and material and all the physics processes involving photons and particles, are implemented using GEANT4. In particular, optical photon processes in a scintillator with complicated geometry can be accurately described by the well-established electromagnetic theory. However, tracking all the optical photons consumes so much time that it is not suitable for massive MC production. Our GEANT4-based model does not track optical photons but uses stored information obtained from the full simulation to ensure both accuracy and speed. It mainly consists of the following parts: transportation of incident particles, scintillation, optical photon processes and PMT response.

3.1. Transportation of incident particles

The configuration of all the geometries and materials of the BESIII detector is implemented in BOOST. Information about incident particles is recorded in discrete steps along their trajectories and both step size and energy loss are calculated automatically in GEANT4, based on various interaction models. Thus both the flight time (t_{flight}) and energy deposition in the scintillator can be obtained.

3.2. Process of scintillation

The luminescence of a scintillator in response to the passage of charged particles is approximately proportional to the energy deposition. A non-linear effect known for high-density ionization is described by the semi-empirical Birks' Law [18]:

$$\frac{d\mathcal{L}}{dx} = \mathcal{L}_0 \frac{dE/dx}{1+\kappa_B\, dE/dx} \tag{1}$$

where $\mathcal{L}$ is the luminescence, and $\mathcal{L}_0$ is the luminescence (or light yield) at low specific ionization density and the constant $\kappa_B = 0.015$ cm/MeV is taken from Ref. [19].

The photon emission time (t_{emit}), consisting of fast and slow components, can be sampled from the probability density function [20]:

$$E(t_{emit}) = \frac{1}{1+R_\tau}\left(\frac{e^{-t_{emit}/\tau_2} - e^{-t_{emit}/\tau_1}}{\tau_2-\tau_1} + \frac{R_\tau}{\tau_3} e^{-t_{emit}/\tau_3}\right) \tag{2}$$

where τ_1 and τ_2 are constants for the fast components, τ_3 is the time constant for the slow component and R_τ is the ratio between the fast and slow components. The timing of signals is determined by the leading edge discrimination, hence the rise time τ_1 and the decay time τ_2 are important parameters for the TOF simulation. We use $\tau_1 = 0.7$ ns and $\tau_2 = 1.8$ ns, according to the properties of BC404 (see Table 1). The values of $\tau_3 = 14.2$ ns and $R_\tau = 0.27$ are taken from Ref. [20].

Scintillation may occur at any time in a specific step. Thus based on the assumption of uniform probability of scintillation in this step, the term t_{step} corrected to emission time (t_{emit}) can be written as

$$t_{step} = r \times \Delta T \tag{3}$$

where r is a uniform random number from 0 to 1 and ΔT is the time in a step. ΔT is controlled by GEANT4 with a typical value of 0.01 ns.

3.3. Optical photon processes

Physics processes of the optical photons in the scintillator include Rayleigh scattering, medium-boundary interactions and absorption. The cross-section for Rayleigh scattering is small for the plastic scintillator. Boundary processes include reflection and refraction. Absorption follows an exponential behavior with the bulk attenuation length of the scintillator as an input parameter.

Optical photons are emitted isotropically from the point of energy deposition in the scintillator and then propagate to the PMT. The essential considerations are how many photons will eventually reach the photocathode and what their arrival time distribution is. Based on all this information obtained and stored from the full GEANT4 simulation, we can precisely simulate optical photon processes. Since storing the information for every point will require

too much memory, in our model, the scintillator is divided into small cells. Symmetries of the scintillator have been used to reduce the number of cells. After optimizing in the global cylindrical coordinates of BESIII, we choose 43 bins along the $\hat{r}$ axis, six bins along the $\hat{\phi}$ axis and six bins along the $\hat{z}$ axis , a total of 1548 cells in 3 dimensions, as shown in Fig. 2. In each cell, isotropic photons are generated at uniform random positions in the full simulation. Since the reflectivity of the ESR and the quantum efficiency of the PMT vary slowly with wavelength [15,17], we use their average values and generate optical photons with a fixed wavelength (468 nm). Absorption of optical photons is considered in the full GEANT4 simulation; the bulk attenuation length for the scintillator BC404 is 1600 mm (see Table 1). The SMOOTH mode in GEANT4 is used for the properties of surfaces of scintillators and ESR based on the fact that scintillators are well-polished and it is difficult to perform a direct measurement of the small roughness after assembly.

The probability of photons reaching the photocathode of the PMT (or the photon collection efficiency) in each cell is defined as the ratio of the number of photons reaching photocathode to the number of photons generated in this cell. The propagation time t_{prop} is recorded in GEANT4 and defined as the time starting from the photon generation to the photon's arrival at the photocathode. Propagation is limited to a time window of 20 ns. The information described above is stored as a look-up table, indexed by the position of a cell and recording the photon collection efficiency and propagation time distribution. Fig. 3 shows a typical propagation time spectrum in a cell. The phenomenon that several peaks exist in the time spectrum is caused by the complicated geometry of the scintillator, where multiple reflections between the 45-degree slope in the end near the PMT and other boundaries.

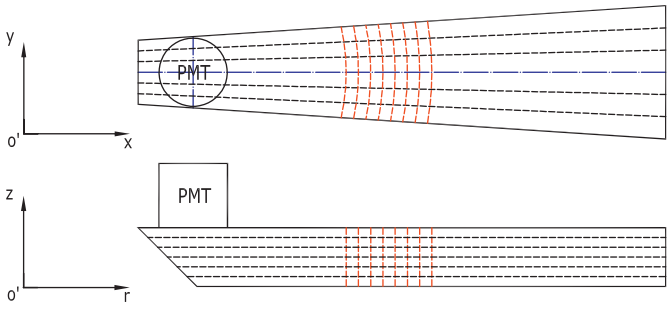

Fig. 2. Partitioning of the endcap TOF geometry in 3 dimensions.

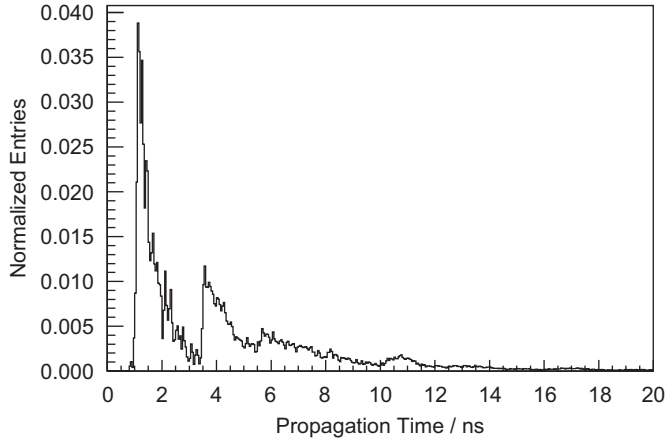

Fig. 3. A typical propagation time distribution of optical photons in a cell.

3.4. PMT response

Since the fine-mesh structure of the PMT R5924 has a good pulse linearity in the probable output current region [15], the PMT output pulse height can be obtained by summing up all the signals from single photoelectrons $v_i(t)$,

$$V_{\mathrm{PMT}}(t) = \sum_{i=1}^{N_{pe}} v_i(t). \tag{4}$$

The final output signal is determined by including the preamplifier as

$$V_f(t) = G_{pre}\, V_{\mathrm{PMT}}(t) \tag{5}$$

where $G_{pre}(=10)$ is the gain of the preamplifier. The time t of a photoelectron at anode is given by

$$t = t_{flight} + t_{emit} + t_{step} + t_{prop} + t_{transit}. \tag{6}$$

The photon propagation time t_{prop} is sampled from the stored distribution (see Fig. 3). $t_{transit}$ is the transit time of the PMT R5924, which is sampled from a Gaussian distribution with a mean of $\bar{t}_{transit} = 9.5$ ns and a sigma of $\sigma_{transit} = 0.187$ ns (see Table 2). The number of photoelectrons N_{pe} is determined from the number of optical photons, the photocathode quantum efficiency and the electron collection factor of the first dynode. Since the quantum efficiency does not change much with wavelength in the photon spectrum ranging from 390 to 500 nm (for BC404 [14]), we use its average value of 22.4% in this model.

The time response function of a single photoelectron [6] is introduced in order to simulate the time-walk effect due to leading edge discrimination scheme applied in the BESIII TOF system,

$$v_i(t) = G_0\, C_e\, \frac{t^2 e^{-t^2/2\tau^2}}{\int t^2 e^{-t^2/2\tau^2}\, dt} \tag{7}$$

where G_0 is the gain of the PMT at a certain high voltage, C_e is a factor to convert charge to voltage and τ is a constant related to the rise time. $\tau = 3.0$ ns is determined by fitting the output pulse (without preamplifier) of the PMT R5924.

We use 125 and 500 mV for the low-level (LL) and high-level (HL) threshold, respectively, which are the same values as the experimental data. The signal timing (TDC) is determined by the moment when the PMT pulse crosses the LL threshold only if the peak of the pulse height is larger than the HL threshold.

The charge (time-to-charge converter (QTC)) is determined by the time integral of the $V_f(t)$ and the resistance in the non-gated QTC circuit $R_f = 61\ \Omega$ [21],

$$QTC = \frac{\int V_f(t)\, dt}{R_f}. \tag{8}$$

3.5. Comparison of the simulation model and the full GEANT4 simulation

We have compared our simulation model with the full GEANT4 simulation in the global BESIII coordinate system. Muons (μ^-) with

Table 2
The property of Hamamatsu PMT R5924.

Photocathode diameter	Electron collection factor	Quantum efficiency (Average)	Rise time
39 mm	0.6	22.4%	2.5 ns
Transit time	Transit time spread (FWHM)	Gain at 1.0 T	
9.5 ns	0.44 ns	2.0×10^5	

a momentum of 1.0 GeV/c travel from the IP towards different positions of the endcap TOF. Four typical values of the polar angle (θ) are chosen by radius (R) positions of the first hit in the scintillator, $R=500, 600, 700$ and 800 mm. The azimuthal angle ϕ is uniformly distributed in the range (1.25°, 6.25°).

Figs. 4 and 5 show the results of QTC and TDC distributions from the two simulations. We can see that at different hit positions, the simulation model can reproduce the results from the full GEANT4 simulation. For one track hitting a scintillator, the average CPU time is 5 s from the full simulation (Intel© Xeon© E5430@2.66 GHz); the corresponding time is reduced to 0.1 s in our model, indicating that the speed of this simulation model is nearly 50 times faster than the full simulation.

4. Comparison with BESIII experimental data

Using the simulation model, we generate MC samples and compare them with the experimental data collected with the BESIII detector at the BEPCII operating at the $J/\psi(1S)$ resonance ($\sqrt{s}=3.097$ GeV). Both the simulation sample and experimental

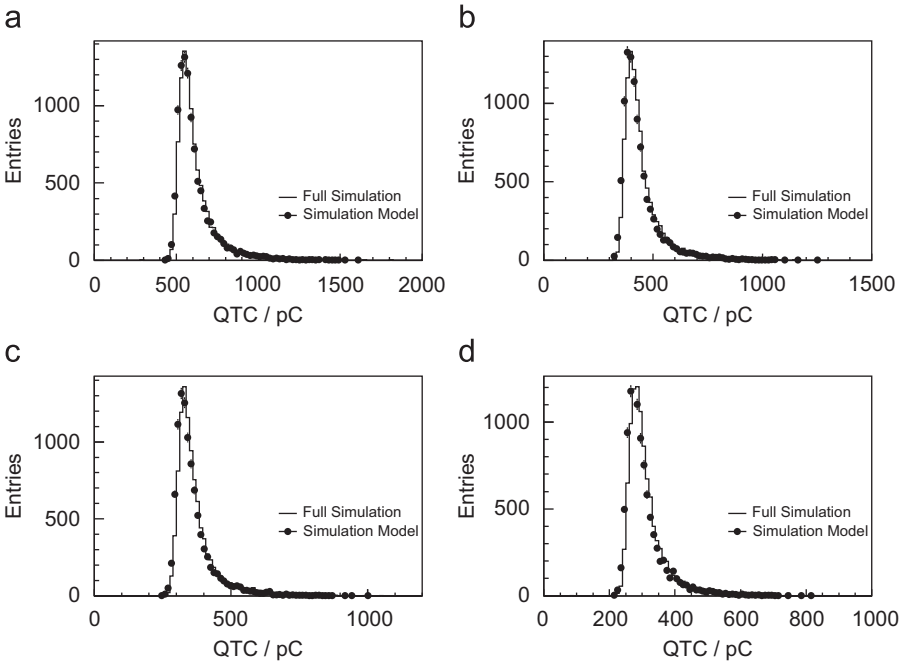

Fig. 4. Compared QTC distributions at different hit positions: (a) $R=500$ mm, (b) $R=600$ mm, (c) $R=700$ mm, (d) $R=800$ mm.

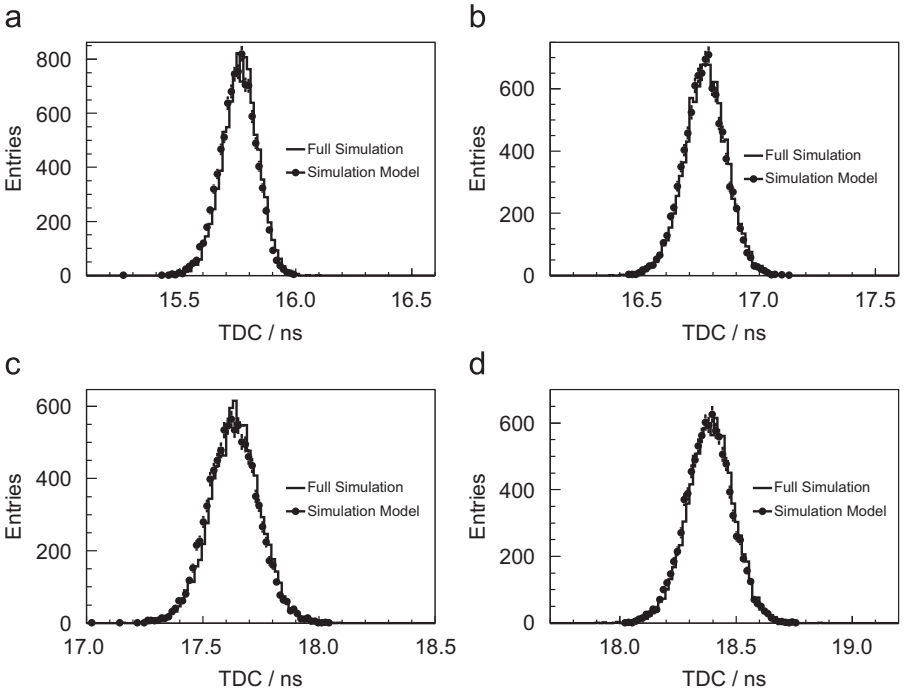

Fig. 5. Compared TDC distributions at different hit positions: (a) $R=500$ mm, (b) $R=600$ mm, (c) $R=700$ mm, (d) $R=800$ mm.

data are fully reconstructed in the BESIII Offline Software System (BOSS) [22].

The TOF reconstruction efficiency is an important parameter for experimental data and MC, which is defined by

$$\varepsilon \equiv \frac{N_{tof}}{N_{ext}} \tag{9}$$

where N_{tof} is the number of reconstructed tracks with $|T^{correct}_{mea} - T_{exp}| \leq 1.5$ ns, $T^{correct}_{mea}$ is the weighted average of measured times after the calibration correction, T_{exp} is the expected time of flight and N_{ext} is the number of extrapolated tracks which can hit the endcap TOF. Both T_{exp} and hit positions (R-hit) are determined by Kalman filter tracking and extrapolation in the Main Drift Chamber (MDC) [1]. Bhabha samples ($e^+e^- \to e^+e^-$) are used since they offer high statistics for the endcap TOF. Reconstruction efficiencies at different hit positions for experimental data and MC are shown in Fig. 6.

The time resolution is another key parameter of the TOF system, determined by a symmetric Gaussian fit to $\delta t = T^{correct}_{mea} - T_{exp}$. Dimuon events ($e^+e^- \to \mu^+\mu^-$) reflect the intrinsic time resolution performance of the endcap TOF because muons interact much less than other particles whilst passing through the complicated material located in front of the endcap TOF. Time resolutions at different hit positions for experimental data and MC are shown in Fig. 7.

For both reconstruction efficiency (Fig. 6) and time resolution (Fig. 7), the MC simulation agrees with experimental data.

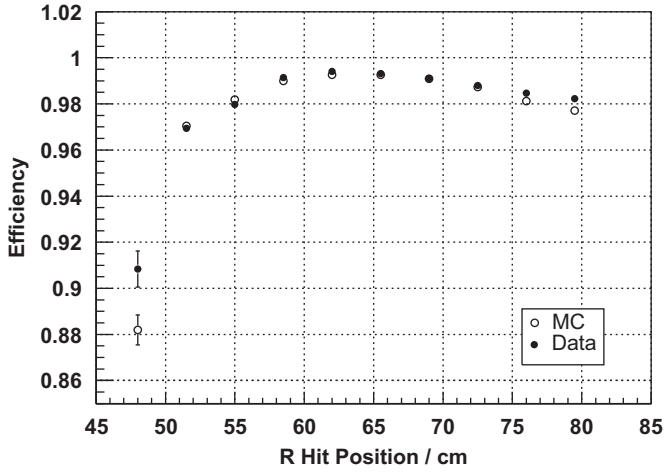

Fig. 6. TOF reconstruction efficiencies at different hit positions.

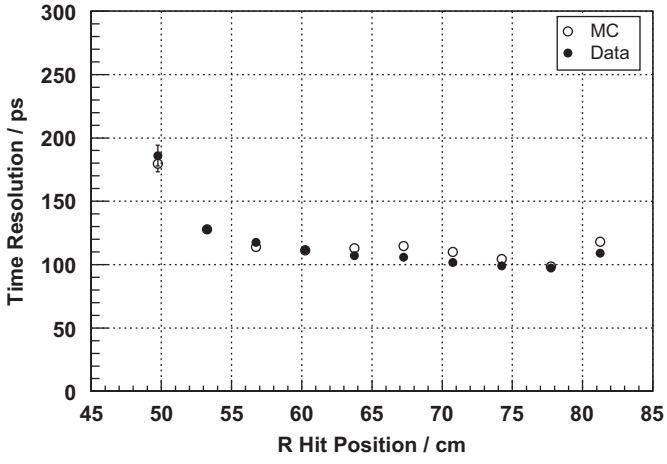

Fig. 7. Time resolutions at different hit positions.

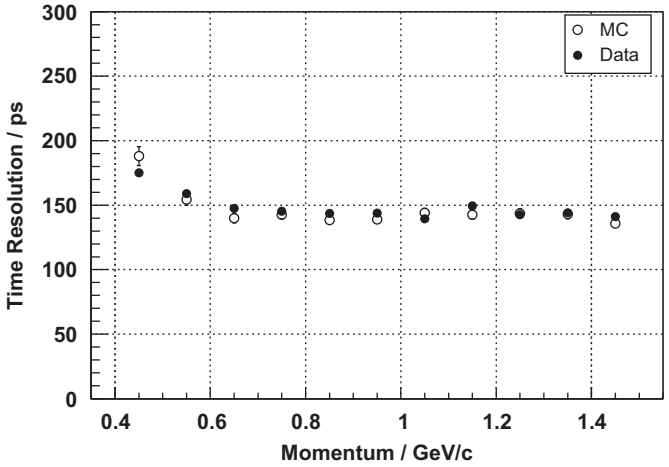

Fig. 8. Time resolutions in different momentum regions.

The discrepancy of the reconstruction efficiency between data and MC occurs at hit radii smaller than 60 cm, which is possibly due to inefficient or poor tracking for charged particles with small polar angles in the MDC.

The time resolution for hadrons is also compared using pions from $J/\psi \to \rho\pi$. Fig. 8 shows the variation of time resolution with momentum. Nice agreement can be seen between experimental data and MC.

5. Conclusion

We have developed a GEANT4-based MC simulation model, which has proved to be reliable and fast in fully simulating the optical photon processes in a complicated geometry. Using the stored information of optical photons instead of tracing each optical photon, this model accelerates simulation by about a factor of 50 compared to the full GEANT4 simulation. It will also be beneficial in other cases where the geometry of scintillators is irregular and high speed and precision of simulation are required. For a system consisting of many different scintillators, the required disk space may be large, since light propagation information has to be stored for each scintillator.

Acknowledgements

We are grateful to the GEANT4 collaboration for their continuous development of the simulation toolkit. We also would like to thank the tremendous efforts of BESIII collaboration and BEPCII accelerator group. This work is supported in part by the Ministry of Science and Technology of China under Contract no. 2009CB825200; the Chinese Academy of Sciences (CAS) Large-Scale Scientific Facility Program; CAS under Contracts nos. KJCX2-YW-N29, KJCX2-YW-N45; Innovation Foundation for Youths of Institute of High Energy Physics under Contract no. H95461C0U2.

References

[1] M. Ablikim, et al., BESIII Collab., Nucl. Instr. and Meth. A 614 (2010) 345.
[2] K.T. Chao, Y.F. Wang, Int. J. Mod. Phys. A 24 (Suppl. 1) .
[3] M. Ablikim, et al., BES Collab., Nucl. Instr. and Meth. A 552 (2005) 344.
[4] S. Agostinelli, et al., GEANT4 Collab, Nucl. Instr. and Meth. A 506 (2003) 250.
[5] J. Allison, et al., IEEE Trans. Nucl. Sci. NS-53 (2006) 270.
[6] J.W. Nam, et al., Nucl. Instr. and Meth. A 491 (2002) 54.
[7] X. Li, et al., High Energy Phys. Nucl. Phys. 29 (2005) 586 (in Chinese).
[8] Z.B. Tang, et al., High Energy Phys. Nucl. Phys. 30 (2006) 445 (in Chinese).
[9] S.H. An, et al., High Energy Phys. Nucl. Phys. 29 (2006) 775.

[10] J. Tickner, G. Roach, Nucl. Instr. and Meth. B 263 (2007) 149.
[11] A. Glazov, N. Raičević, A. Zhokin, Comput. Phys. Commun. 181 (2010) 1008.
[12] E. Barberio, et al., J. Phys. Conf. Ser. 160 (2009) 012082.
[13] Z.Y. Deng, et al., High Energy Phys. Nucl. Phys. 30 (2006) 371 (in Chinese).
[14] Data sheet for BC-404 at Saint-Gobain Crystals & Detector website, 〈http://www.detectors.saint-gobain.com/uploadedFiles/SGdetectors/Documents/Product_Data_Sheets/BC400-404-408-412-416-Data-Sheet.pdf〉.
[15] Handbook of Hamamatsu: Fine-mesh PMT series for high magnetic field environments, 〈http://sales.hamamatsu.com/assets/applications/ETD/pmt_handbook_complete.pdf〉.
[16] Data sheets for BC-634A at Saint-Gobain Crystals & Detector website, 〈http://www.detectors.saint-gobain.com/uploadedFiles/SGdetectors/Documents/Brochures/Organics-Brochure.pdf〉.
[17] C. Wu, et al., Nucl. Instr. and Meth. A 555 (2005) 142.
[18] J.B. Birks, Proc. Phys. Soc. London Sect. A 64 (1951) 874.
[19] R.L. Craun, D.L. Smith, Nucl. Instr. and Meth. 80 (1970) 239.
[20] C.M. Hawkes, et al., Nucl. Instr. and Meth. A 292 (1990) 329.
[21] S.B. Liu, et al., Nucl. Instr. and Meth. A 621 (2010) 513.
[22] W. Li, et al., The offline software for the BESIII experiment, in: The Proceedings of CHEP06, Mumbai, 2006.